Environmental Pollution 374 (2025) 126254

Contents lists available at ScienceDirect

Environmental Pollution

journal homepage: www.elsevier.com/locate/envpol

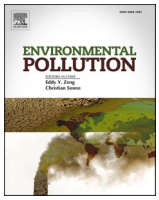

Properties of inflowing Pacific and Atlantic water govern total and methylated mercury profiles in the Arctic Ocean☆

Sangwoo Eom [a], Anne L. Soerensen [b], Tae Siek Rhee [c], Jong Kuk Hong [d], Purena Son [e], Tae Keun Rho [e], Seunghee Han [a,*]

[a] Department of Environment and Energy Engineering, Gwangju Institute of Science and Technology (GIST), Gwangju, 61005, Republic of Korea
[b] Department of Environmental Monitoring and Research, Swedish Museum of Natural History, Stockholm, 11418, Sweden
[c] Division of Ocean and Atmospheric Sciences, Korea Polar Research Institute (KOPRI), Incheon, 21990, Republic of Korea
[d] Division of Glacier and Earth Sciences, Korea Polar Research Institute (KOPRI), Incheon, 21990, Republic of Korea
[e] Marine Environmental Research Department, Korea Institute of Ocean Science and Technology (KIOST), Busan, 49111, Republic of Korea

ARTICLE INFO

Keywords:
Total mercury
Methylmercury
Biological index
Chlorophyll-a
Canada Basin
Pacific water

ABSTRACT

High methylmercury (MeHg) concentrations in Arctic marine biota have been linked to high MeHg uptake driven by shallow MeHg peaks at water depths of 100–300 m in the Arctic Ocean. To understand how the biogeochemical characteristics of each basin affects the distribution of total Hg (THg) and MeHg across the Arctic Ocean, the spatial patterns of THg and MeHg were investigated using data from new transects in the Beaufort Sea (BS) and previously published Arctic Ocean expeditions covering the Canada Basin and Makarov Basin in the Pacific sector, and Amundsen Basin and Nansen Basin in the Atlantic sector. In the BS, the THg concentration in the polar mixed water increased with salinity ($r = 0.87$, $p < 0.01$), which was linked to THg transport from the Chukchi Shelf. Transport of Hg from the Chukchi Shelf also drove elevated THg concentrations in the polar mixed water and halocline water in the Canada Basin and Makarov Basin compared to other Arctic basins. The MeHg concentration in the BS was positively correlated with the biological index in the Pacific summer water ($r = 0.86$, $p < 0.01$), demonstrating that intrusion of warm and nutrient-rich Pacific water promotes MeHg production in the BS. In line with this result, chlorophyll-a showed a comparable cross-basin trend to that of MeHg, with the highest values in the Nansen Basin. In the halocline water, MeHg concentrations were highest in the Canada Basin likely due to the largest availability of Hg(II). On the contrary, MeHg concentration was highest in the Nansen Basin in the Atlantic water layer, which could be related to the higher seawater temperature and enhanced biological production. The results of this study underscore the critical role of Pacific and Atlantic inflows in modulating the profiles of THg and MeHg in the Arctic Ocean.

1. Introduction

Mercury (Hg) levels in Arctic marine mammals and indigenous people are notably higher than those in other regions, resulting in the highest Hg concentrations in human blood globally (Basu et al., 2022). This phenomenon may be related to elevated concentrations of methylmercury (MeHg) in the upper part (100–300 m) of the Arctic Ocean (Heimbürger et al., 2015; Kim et al., 2020) as well as low biodilution associated with low biological production found in the Arctic Ocean (Basu et al., 2022; Lavoie et al., 2013). MeHg in Arctic seawater consists of monomethylmercury (MMHg) and dimethylmercury (DMHg) (Black et al., 2009; Jonsson et al., 2022a; Petrova et al., 2020). While a wide range of DMHg/MeHg ratio has been reported in the Arctic Ocean (Agather et al., 2019; Jonsson et al., 2022a; Petrova et al., 2020), *in situ* methylation of Hg(II) in the subsurface layer, producing MMHg via microbial remineralization of sinking particulate organic carbon (POC), appears to be the largest source of MeHg in Arctic seawater (Heimbürger et al., 2015; Jonsson et al., 2022b), equivalent to the combined inputs from river discharge, atmospheric deposition, and sediment transport (Lehnherr et al., 2011; Petrova et al., 2020).

Pacific water (PW), which is fresher than Atlantic water (AW), enters the Arctic Ocean through the shallow (50-m water depth) Bering Strait,

☆ This paper has been recommended for acceptance by Sarah Harmon.

* Corresponding author.
E-mail address: shan@gist.ac.kr (S. Han).

https://doi.org/10.1016/j.envpol.2025.126254
Received 7 October 2024; Received in revised form 9 April 2025; Accepted 13 April 2025
Available online 15 April 2025

and then, it moves toward the subsurface layer of the East Siberian Sea, Chukchi Sea, and Canada Basin (Fig. 1) (Brugler et al., 2014). On the other hand, warm, saline AW enters the Arctic Ocean through the Barents Sea Opening (bottom depth ~400 m) and the Fram Strait (bottom depth ~2600 m). As AW moves toward the north, a cyclonic gyre is formed on the Nansen Basin, while an anticyclonic gyre is formed on the Canada Basin by wind-driven Ekman transport. Between these two circulations, Transpolar Drift crossing the Arctic Ocean carries PW, sea ice, and Siberian shelf water toward the Greenland Sea and Baffin Bay (Liguori et al., 2021; Rudels and Carmack, 2022). Due to this surface circulation pattern, the volume transport ratio of AW to PW is ~1 in the Amerasian Basin, while it is much higher in the Eurasian Basin, at ~5–8, for the entire water depth (Bluhm et al., 2015). This difference results in distinct water mass structures between two basins: the surface mixed layer depth in the Amerasian Basin averages ~8 m in summer and ~30 m in winter, which is much shallower than the surface mixed layer depth of the Eurasian Basin, at ~20 m in summer and 70–100 m in winter (Peralta-Ferriz and Woodgate, 2015). The strong stratification, which is related to the inflow of low-salinity PW, in the Amerasian Basin inhibits upward nitrate flux from the subsurface to the polar mixed water (PMW), leading to relatively low net community production, as compared to in the Eurasian Basin, particularly during summer, when brine-driven vertical mixing is limited (Codispoti et al., 2013; Randelhoff et al., 2020). Using the reference data accumulated from 2007 to 2017, Randelhoff et al. (2020) showed that the turbulent flux of nitrate, which is lower in the Arctic Ocean than in other oceans by one to two orders of magnitude, was even lower in the Amerasian Basin than in the Eurasian Basin, leading to the higher primary production in the Eurasian Basin. However, primary production and nitrate assimilation in the subsurface seawater are higher in the Amerasian Basin than in the Eurasian Basin due to the inflow of warm, productive Pacific Summer Water (PSW) (MacKinnon et al., 2021). These physical properties may create distinctive MeHg profiles for the Amerasian and Eurasian Basins.

In the Arctic Ocean, the MeHg concentration is relatively low in the surface layer due to photodemethylation, biological uptake, and atmospheric evasion, while it is enriched in the subsurface layer due to *in situ* methylation (Baya et al., 2015; Petrova et al., 2020). For *in situ* methylation, the water mass properties have been suggested to be critical (Agather et al., 2019; Wang et al., 2018). For example, MeHg concentration maxima in the water column decrease across the Canadian Arctic Archipelago as one moves east, attributable to the increased *in situ* methylation in the western sea as a consequence of the lateral transport of nutrients-enriched halocline water from the Chukchi Shelf and Beaufort Shelf (Wang et al., 2018). The importance of *in situ* methylation compared to advection of preformed MeHg is also supported by the result of a central Arctic Ocean survey, which showed no clear correlations between MeHg concentration and apparent oxygen utilization being advected from the productive shelves (Agather et al., 2019). A comparable MeHg distribution was reported across the entire water depth of the Barents Sea, except for the MeHg maximum at water depths of 80–120 m in the Nansen Basin where AW-influenced warm water mass is observed (Kohler et al., 2022). While these previous reports commonly highlight the importance of the biogeochemical properties of seawater for *in situ* MeHg production, the critical properties governing distinctive vertical MeHg profiles across the Arctic basins remain understudied.

In this study, we examine how the biogeochemical conditions of each basin affect the distribution of total Hg (THg) and MeHg across the Arctic Ocean. We first explore the vertical and horizontal distributions of THg, MeHg, fluorescent dissolved organic matter (DOM), and conventional water parameters (salinity, temperature, dissolved oxygen, fluorescence, NO_3^-, PO_4^{3-}, $Si(OH)_4$, and dissolved organic carbon [DOC]) at nine sites in the Beaufort Sea (BS) from August to September 2022 (Fig. 1). Using the measured values, we discuss the water mass structures and biogeochemical conditions that are important for the transport of THg and the production and decomposition of MeHg. We then extend the findings from the southern BS to the entire Arctic Ocean using datasets from other Arctic expeditions (i.e., the GEOTRACES, ARA09C, TransArc [ARK-XXVI/3], SWEDARCTIC, 2016, and COMIDA CAB projects) (Table S1), with an emphasis on the effect of PW and AW inflows on the cross-basin profiles of THg and MeHg.

2. Materials and methods

2.1. Seawater sampling

Seawater samples were collected using a rosette sampling system with acid-cleaned 10 L Niskin bottles in the southern BS during the ARA13C expedition from August 26 to September 7, 2022 (Fig. 1). Sampling locations were selected in the western (W01–W05) and eastern (E01–E04) transects to identify the effect of the Mackenzie River plume and PW inflow on THg and MeHg distributions. In general, PW inflow is stronger in the western transect, and the Mackenzie River plume is stronger in the eastern transect due to the prevailing wind

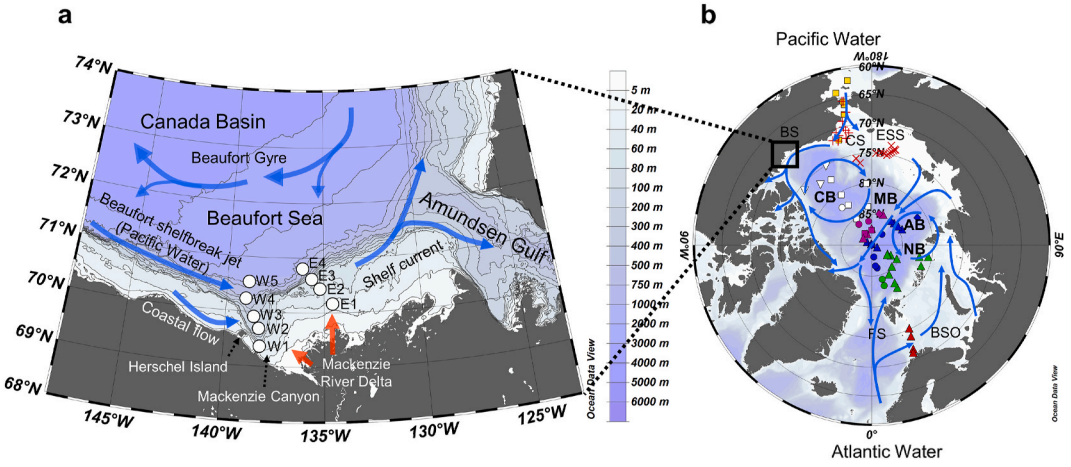

Fig. 1. (a) Location of the seawater sampling sites in the southern BS during the ARA13C expedition. (b) The sampling sites of the GN01 (square), GN03 (inversed triangle), GN04 (triangle), SWEDARCTIC 2016 (circle), ARK-XXVI/3 (diamond), ARA09C (X), and COMIDA CAB (crossed) expeditions. The data of the red and yellow sites are shown in Fig. 2, and the data of the other sites are shown in Figs. 3–5 and S10. CB sites are shown in white, MB sites are purple, AB sites are blue, and NB sites are green. CB: Canada Basin; MB: Makarov Basin; AB: Amundsen Basin; NB: Nansen Basin; CS: Chukchi Sea; ESS: East Siberian Sea; BS: Beaufort Sea; BSO: Barents Sea Opening; FS: Fram Strait. (For interpretation of the references to colour in this figure legend, the reader is referred to the Web version of this article.)

direction (Ehn et al., 2019). At each station, we selected water sampling depths based on the temperature, dissolved oxygen, and fluorescence profiles obtained *in situ* using a conductivity-temperature-depth (CTD) probe (SBE 911plus) and other sensors onboard the R/V Araon. Water treatment methods for the analysis of Hg and other parameters are available in Text S1.

For the cross-Arctic analysis of Hg, we used published Arctic Hg datasets derived from the GEOTRACES (GN01, GN03, and GN04), ARA09C, TransArc (ARK-XXV I/3), SWEDARCTIC 2016, and COMIDA CAB projects (Table S1). We excluded filtered MeHg observations due to the loss of particulate MMHg and DMHg during filtration (West et al., 2023). We used salinity and temperature obtained from the GEOTRACES intermediate data products (GN01 and GIPY11) for the water property analysis (Schlitzer and Mieruch-Schnülle, 2024). Chlorophyll-a (Chl-a) data were obtained from the GN01, GN03, GN04, and ARK-XXVI/3 surveys, and nutrient data were obtained from the GN01 and GIPY11 surveys.

2.2. Seawater analysis

Analytical methods and quality assurance data for THg and MeHg are available in Text S2. The filtered samples used for DOC analysis were initially acidified with 1 % HCl (v/v). Before measurement, they were purged with high-purity N_2 for 8 min to remove dissolved inorganic carbon. The amount of DOC was measured using high temperature combustion (850 °C) to convert the DOC into CO_2, which was quantitatively determined by means of a nondispersive infrared detector with a Pt catalysis (VarioTOC, Elementar). The NO_3^-, PO_4^{3-}, and $Si(OH)_4$ in the seawater samples were measured using a Nutrient AutoAnalyzer (QuAAtro, Seal Analytical, USA) at the Korea Institute of Ocean Science and Technology.

The excitation emission matrix (EEM) fluorescence spectra were employed to measure the qualitative properties of the DOM. To mitigate the inner filter effect, the sample was diluted to reduce the absorption coefficient to <10 m^{-1} (Stedmon and Bro, 2008). A Hitachi F-2500 fluorescence spectrophotometer (Hitach High Technologies, Japan) operating in scan mode with a Xenon lamp was used to obtain the EEM spectra for all the seawater samples and the Milli-Q water. The measurements were conducted in a 1-cm quartz cuvette at an ambient temperature. The emission (Em) wavelength ranged from 280 nm to 550 nm in 2-nm increments, and the excitation (Ex) wavelength ranged from 220 nm to 500 nm in 5-nm increments, with a scan speed of 3000 nm min^{-1}. To eliminate potential artifacts due to Rayleigh and Raman scattering, the fluorescence spectrum of the Milli-Q water was subtracted from the spectra of the seawater samples (Stedmon et al., 2003). To identify the origin of DOM, we utilized EEM fluorescence spectra and calculated the biological index (BIX) and humification index (HIX) as follows (Hansen et al., 2016):

$$BIX = \frac{Em\ 380\ nm}{Em\ 430\ nm} \text{ at Ex 310 nm}$$

$$HIX = \frac{Peak\ area\ under\ the\ Em\ (435-480\ nm)}{Peak\ area\ under\ the\ Em\ (300-345\ nm) + Peak\ area\ under\ the\ Em\ (435-480\ nm)} \text{ at Ex 254 nm}$$

The oxygen isotope ratios ($\delta^{18}O$) obtained from the GN01 and GN03 expeditions were used to identify the relative contributions of sea ice meltwater (SIM), meteoric water (MW), and PW using the equations below (Pasqualini et al., 2017; Schlitzer and Mieruch-Schnülle, 2024).

$$1 = f_{SIM} + f_{MW} + f_{PW}$$

$$S = f_{SIM}S_{SIM} + f_{MW}S_{MW} + f_{PW}S_{PW}$$

$$\delta^{18}O = f_{SIM}\delta^{18}O_{SIM} + f_{MW}\delta^{18}O_{MW} + f_{PW}\delta^{18}O_{PW}$$

where f and S are the fraction of water mass and salinity, respectively. The end-member values of salinity and $\delta^{18}O$ used for the calculation above are listed in Table S2.

2.3. Statistical analysis

Pearson correlation analyses were used to investigate the relationship between Hg species and water parameters. A one-way ANOVA supplemented with a post-hoc Duncan's test was used to compare THg and MeHg concentrations across the Arctic basins. Interquartile range (IQR), or the difference between the first quartile (Q1) and the third quartile (Q3) of the dataset, was used to determine outliers (Streit and Gehlenborg, 2014), and extreme values lower than Q1 – (1.5 × IQR) or higher than Q3 + (1.5 × IQR) were excluded from the datasets. The number of outliers is 65, accounting for 8.7 % of the total dataset (n = 744). Before the ANOVA was performed, data normality was tested using a Shapiro–Wilk test. To meet the normality assumption, variables were log-transformed when necessary. The statistical significance was verified at $p < 0.05$. All statistical analyses were performed using the IBM SPSS package 20.0 (IBM, USA) and Sigma Plot 12.0 software.

3. Results and discussion

3.1. Water mass identification in the Beaufort Sea

Water masses in the BS were identified, following the literature, as upper polar mixed water (UPMW), lower polar mixed water (LPMW), upper halocline water (UHW), lower halocline water (LHW), and AW (Matsuoka et al., 2012) (Table S3; Fig. S1). The relatively low salinity in the UPMW (<~20 m) is mainly attributed to the Mackenzie River inflow, rather than sea ice melting, as shown by the negative relationship between temperature and salinity (Fig. S1) and the lack of sea ice during the sampling period (Fig. S2). The water mass identification study, using ^{127}I and ^{129}I data collected in the BS from August 12 to September 29, 2022 (MR22-06C survey), reported that the major freshwater source for the PMW of the BS is river water, rather than meltwater (Qi et al., 2024). The LPMW (~20–30 m) is considered remnant winter PMW formed by the convection of cold water generated from sea ice formation (Peralta-Ferriz and Woodgate, 2015). The UHW found water depths of ~30–200 m includes PSW and Pacific Winter Water (PWW; Fig. S1). The PSW, observed in the upper layer of the UHW, originates from Alaskan coastal water and Chukchi Shelf water, which transport heat and freshwater to the BS via the Beaufort shelf-break jet (Brugler et al., 2014). This notion is supported by the highest temperature being observed for W5 (0.30 °C), the most northerly site of the western transect (Figs. S1 and S3). The PWW originates from newly ventilated seawater via the convective sinking of brine during sea ice formation on the Chukchi Sea and northern Bering Shelf (Lin et al., 2023). LHW (~200–400 m) is formed by the diapycnal mixing of lower PWW and upper AW and has relatively low dissolved oxygen levels, at 256–262 μmol kg^{-1} (Fig. S3). The dissolved oxygen values observed in the LHW were slightly lower than the previously reported value (270 μmol kg^{-1}) for the Canada Basin (Alkire et al., 2010). The salinity range

of the AW, which is located below a water depth of ~400 m, was higher than 34.7, and the temperature range was 0.17–0.73 °C (Table S3).

3.2. Biogeochemical properties of the Beaufort Sea

The fluorescence and DOC maxima in the UPMW were found along the Mackenzie River plume, which was identified by the higher temperature and lower salinity as compared to the surrounding water (Fig. S4). The subsurface fluorescence maxima were found in the upper UHW, which includes PSW. In particular, the fluorescence maximum in the PSW was found at W5, suggesting that newly transported warm PW created biologically productive conditions in the western BS (MacKinnon et al., 2021). Phosphate and silicate maxima were commonly observed in the lower UHW, which consists of PWW (Fig. S5). In winter, brine-driven convective overturning and wind effects transport dissolved nutrients from sediment to the overlying water on the northern Bering Sea and Chukchi Shelves, and this may cause the phosphate and silicate enrichment in the PWW in the western BS (Dabrowski et al., 2022). In the eastern BS, shelf and slope sediment appears to be a primary source of phosphate and silicate in the PWW based on their vertical profiles, as was observed for dissolved Fe (Hioki et al., 2014).

The biological index (BIX) is an indicator of recent biological activities producing fresh protein-like DOM, whereas the humification index (HIX) describes the humic substance content or the extent of humification in seawater (DeFrancesco et al., 2023; Hansen et al., 2016). In the PSW and PWW, BIX was generally higher in the west than the east, and HIX was higher in the east than the west (Fig. S6). The PWW in the western transect had higher BIX and lower HIX than that in the eastern transect. This contrast could be the result of the *in situ* production of protein-like DOM in the western BS being influenced by the biologically productive condition in the PSW (MacKinnon et al., 2021).

3.3. THg distribution in the Beaufort Sea

The THg concentration averaged 1.7 ± 0.38 pM (n = 9) in the UPMW and 1.5 ± 0.35 pM (n = 11) in the LPMW (Figs. S7a–d). In the UPMW, the lower concentrations of THg were generally found along the Mackenzie River plume, while the higher concentrations were found at the offshore sites of the western transects. In fact, THg concentrations in the UPMW increased with salinity ($r = 0.87$, $p < 0.01$), excluding W1 (Fig. 2). This trend stands in contrast with the significant negative correlation between THg and salinity ($r = -0.79$, $p < 0.01$) observed in the Chukchi Sea, East Siberian Sea, and Barents Sea (Kim et al., 2020; Petrova et al., 2020). The intrusion of PW modified in the Chukchi Sea could be a significant source of THg in the BS. The THg concentration found in the PMW at W4 and W5 (2.1 pM) with salinity 23–27 was, in fact, comparable to the depth-averaged dissolved Hg concentration (<50 m, 1.2–3.6 pM) found in the eastern Chukchi Sea (Fox et al., 2014) (Fig. 2). The relatively low THg concentrations observed in the Mackenzie River plume could be related to the Hg removal through particle sedimentation in the coastal zone, as THg concentrations declined from the Mackenzie river plume to ~16 % of the original endmember in the inner shelf zone (Graydon et al., 2009). The removal of Hg through particle settling is also supported by the high suspended particulate matter (SPM) concentration (~50 mg L^{-1}) found in the river water, which was linked to the presence of erodible materials within loosely consolidated alluvium sediment, and the high fraction of particle-bound Hg observed in the river water (88 % of THg) (Emmerton et al., 2013; Graydon et al., 2009; Zolkos et al., 2020). The effective removal of Hg related to colloidal flocculation and particle settling has been widely observed in other coastal seawater (Eom et al., 2024; Saniewska et al., 2022; Soerensen et al., 2016b).

The THg concentration in the UHW, including PSW and PWW, was slightly higher at the western sites (1.7 ± 0.35 pM, n = 9) than at the eastern sites (1.4 ± 0.17 pM, n = 6), perhaps due to PW intrusion, as higher values were observed at W5 (Figs. S7a–d). The THg maximum was found at E1 (5.2 pM), where a distinctively high SPM concentration (13 mg L^{-1}), 16-fold higher than the averaged SPM concentration of 0.8 mg L^{-1} (0.0028–4.3 mg L^{-1}, n = 42) for the other sites, was observed (Fig. S4). The elevated SPM in the shelf bottom water may be attributed to the downwelling return flow from the shelf (Ehn et al., 2019). The mass of Hg adsorbed on the suspended sediment in E1, which was obtained by dividing the difference in THg concentrations between E1 and other sites by the corresponding difference in SPM concentrations, was 284 pmol g^{-1}. This value was slightly higher than the range of THg concentrations found in the surface sediment of the BS (160–259 pmol g^{-1}; (Chaudhary et al., 2024), supporting the notion that sediment resuspension could be the main source of Hg for the E1 bottom water.

The THg concentration in the LHW was 1.6 ± 0.080 pM (n = 5) in the western and eastern transects observations (Fig. S7). Particularly high THg concentrations were noted at E3 and E4 on the eastern transect, which appeared to be the sediment release of Hg. High concentrations of Fe, nutrients, humic-like DOM, as well as low N* values related to the

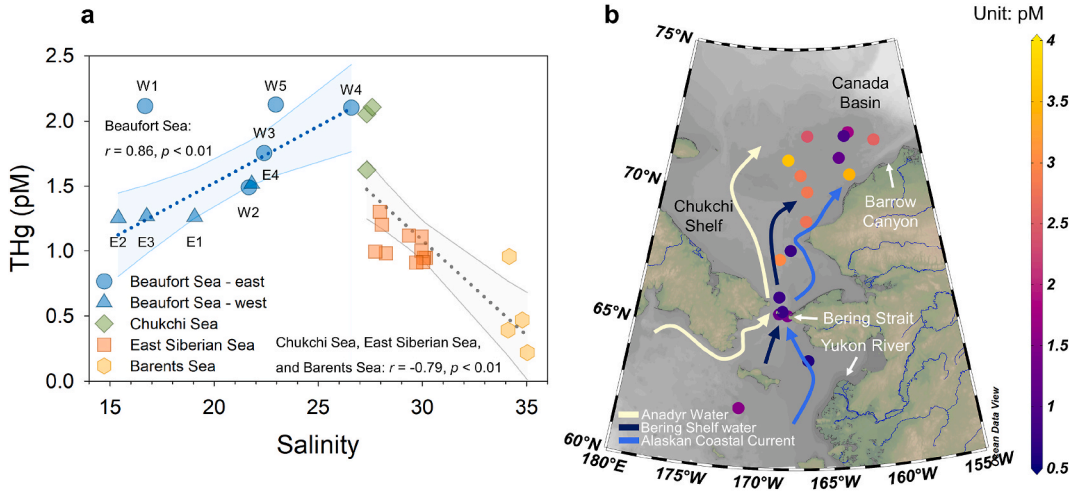

Fig. 2. (a) The relationship between THg concentration and salinity in the west (W1–W5) and east (E1–E4) transects of the BS, Chukchi Sea, East Siberian Sea, and Barents Sea at shallow depths (<10 m). Linear regression models are shown with the best fit (dotted line) and 95 % confidence intervals (shaded). W1 is excluded in the linear regression model for the Beaufort Sea. (b) Dissolved Hg concentrations at the upper layer (<50 m) in the Bering Sea and Chukchi Shelf were obtained from GN01 and COMIDA CAB (Agather et al., 2019; Fox et al., 2014).

sediment release were observed in the shelf and slope bottom water of the Western Arctic Ocean (Hioki et al., 2014). In fact, the release of SPM, phosphate, and silicate from sediment was noted in the LHW of the east transect (Figs. S4 and S5). The THg concentration in the AW was 1.3 ± 0.20 pM (n = 6), significantly lower than that observed in the PMW and halocline water ($p < 0.05$; Fig. S7). The higher THg concentrations in the upper water could be ascribed to the transport of Hg via atmospheric deposition, river discharge, sea ice melt, as well as advection from the Canada Basin and Chukchi Sea (Agather et al., 2019; Jonsson et al., 2022a; Kim et al., 2020, 2023).

3.4. Influence of Pacific water on the cross-Arctic distribution of THg

The water mass of the entire Arctic Basins was categorized into PMW, UHW, LHW, and AW based on modified criteria derived from the literature (Table S4 and Fig. S8). The potential density criterion for the PMW of the Amundsen Basin is the same as that for the UHW of the Makarov Basin due to the deeper mixing in the Amundsen Basin. For the same reason, the potential density criterion for the PMW of the Nansen Basin is close to that for the UHW of the Amundsen Basin. Accordingly, the PMW depth increases from the Pacific sector (~50 m) to the Atlantic sector (~70–120 m) (Fig. S9). Fig. S9 also shows that nutrient-rich PWW, which is characterized by the highest concentrations of NO_3^- (>15 μmol kg^{-1}) and PO_4^{3-} (>1.2 μmol kg^{-1}) and the lowest N* values (<−9.0 μmol kg^{-1}), is found in the UHW of the Canada Basin and the southern Makarov Basin.

The cross-basin comparison of THg concentrations (see individual cruise information in Fig. 1b and Table S1) shows that the THg concentration in the PMW decreased from the Pacific sector to the Atlantic sector in the following order: the Canada Basin (1.7 ± 0.68 pM) > the Makarov Basin (1.6 ± 0.25 pM) > the Amundsen Basin (1.1 ± 0.42 pM) > the Nansen Basin (0.78 ± 0.17 pM), with significant differences being observed between the Amerasian Basin and Eurasian Basin ($p < 0.05$, ANOVA; Fig. 3). Within the Canada Basin, the THg concentration in the PMW was significantly ($p < 0.01$) higher in the open water zone located at 75.0–77.4°N (2.3 ± 0.3 pM, n = 6) than in the sea ice zone located at 80.0–85.1°N (1.5 ± 0.3 pM, n = 7) (Fig. S10) (Agather et al., 2019; Jonsson et al., 2022a; Wang et al., 2018). The THg concentration in the Amundsen Basin was also significantly ($p = 0.048$) higher in the open water zone located at 81.4°N (1.6 ± 0.2 pM, n = 3) than in the sea ice zone located at 84.8–90.0°N (1.1 ± 0.4 pM, n = 44). This result suggests that atmospheric Hg deposition leads to higher THg concentrations in the PMW of the open water zone than the sea ice zone, despite increased Hg evasion flux (Andersson et al., 2008; DiMento et al., 2019; Yue et al., 2023a). The Hg mass budget study also reports that the Hg deposition flux (65 Mg yr^{-1}) to the surface of the Arctic Ocean is higher than the Hg evasion flux (35 Mg yr^{-1}) (Dastoor et al., 2022). The cross-basin trends show a gradual decrease in THg concentrations from the Canada Basin and Makarov Basin to the Nansen Basin in both open water and sea ice zones. Consequently, sea ice content seems to account for the intra-basin trend of THg, while the inter-basin trend of THg cannot be explained. Nonetheless, given the small amount of data used, further investigation is needed to ensure the role of sea ice.

The THg concentrations in the Arctic PMW (0–50 m) increased with decreasing salinity, which implies that freshwater intrusion could be important sources of THg (Fig. 4). Ekman convergence stores a large amount of freshwater from the Mackenzie River, PW, ice meltwater, and precipitation within the Beaufort Gyre in the Canada Basin (Aksenov et al., 2016). The PMW of the Canada Basin can be divided into lower and upper branches in a T-S diagram (Fig. S8a). According to the mixing model constructed using $\delta^{18}O$ data obtained from the literature, the upper branch water, found in the lower layer of the PMW, contains a significantly ($p = 0.03$) smaller fraction of ice meltwater and meteoric water (i.e., runoff and precipitation) (0.11 ± 0.022, n = 7) than the lower branch water (0.15 ± 0.014, n = 3; Table S5). The THg concentration averaged 2.0 ± 1.1 pM (n = 7) in the upper branch and 1.7 ± 0.29 pM (n = 3) in the lower branch, indicating that PW contribution to the Hg concentration in the Canada Basin is larger than that of meltwater and meteoric water. In line with this, Hg flux from the major river and coastal erosion in the Canada Basin (5.1 Mg yr^{-1}) was lower than other basins (8.2–20 Mg yr^{-1}) (Table S6). The depth-averaged dissolved Hg concentration in the Chukchi Shelf is 2.8 ± 1.4 pM, while that in the

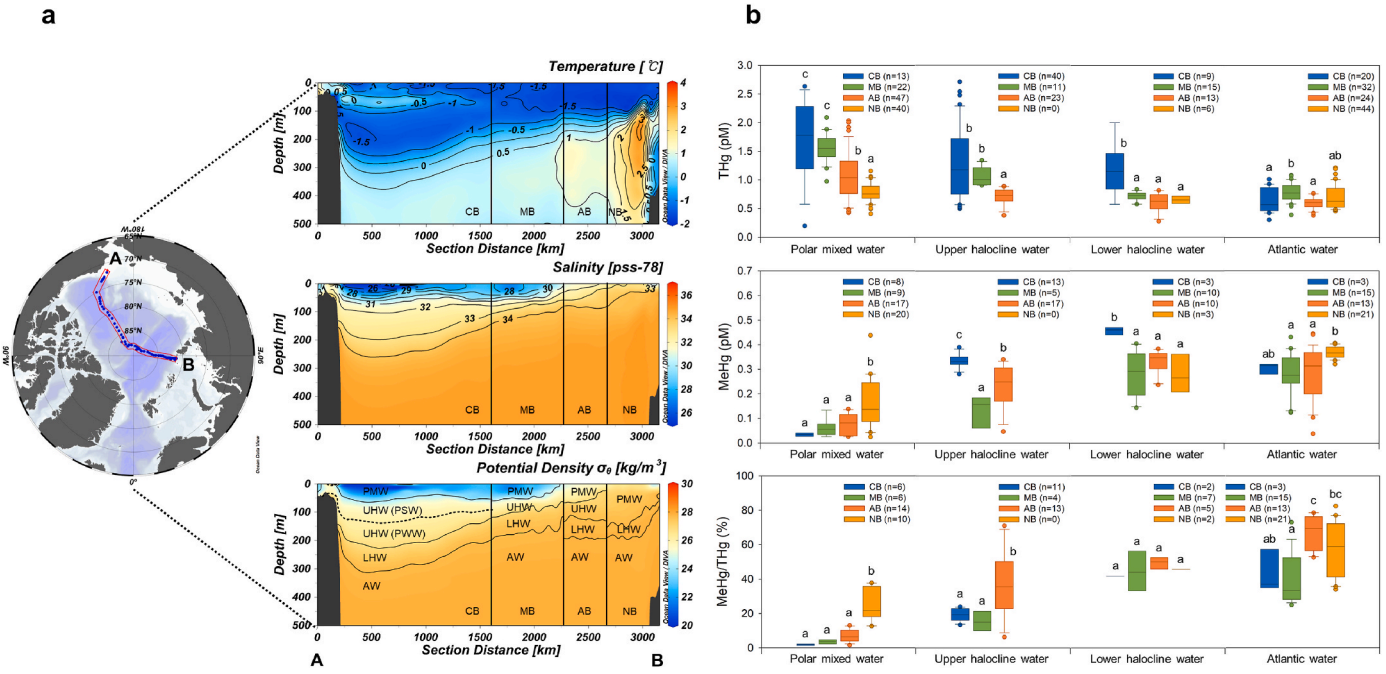

Fig. 3. (a) Temperature and salinity profiles in the upper 500 m layer of the sampling routes of GN01 and GIPY11 expeditions. (b) Box plots show the interquartile range (25th and 75th percentiles), median (black lines), and 10–90 % confidence interval (whiskers) for the THg, MeHg, and MeHg/THg in the Arctic basins. The statistically significant difference between each basin is described with a, b, and c based on post-hoc Duncan method. CB: Canada Basin, MB: Makarov Basin, AB: Amundsen Basin, and NB: Nansen Basin.

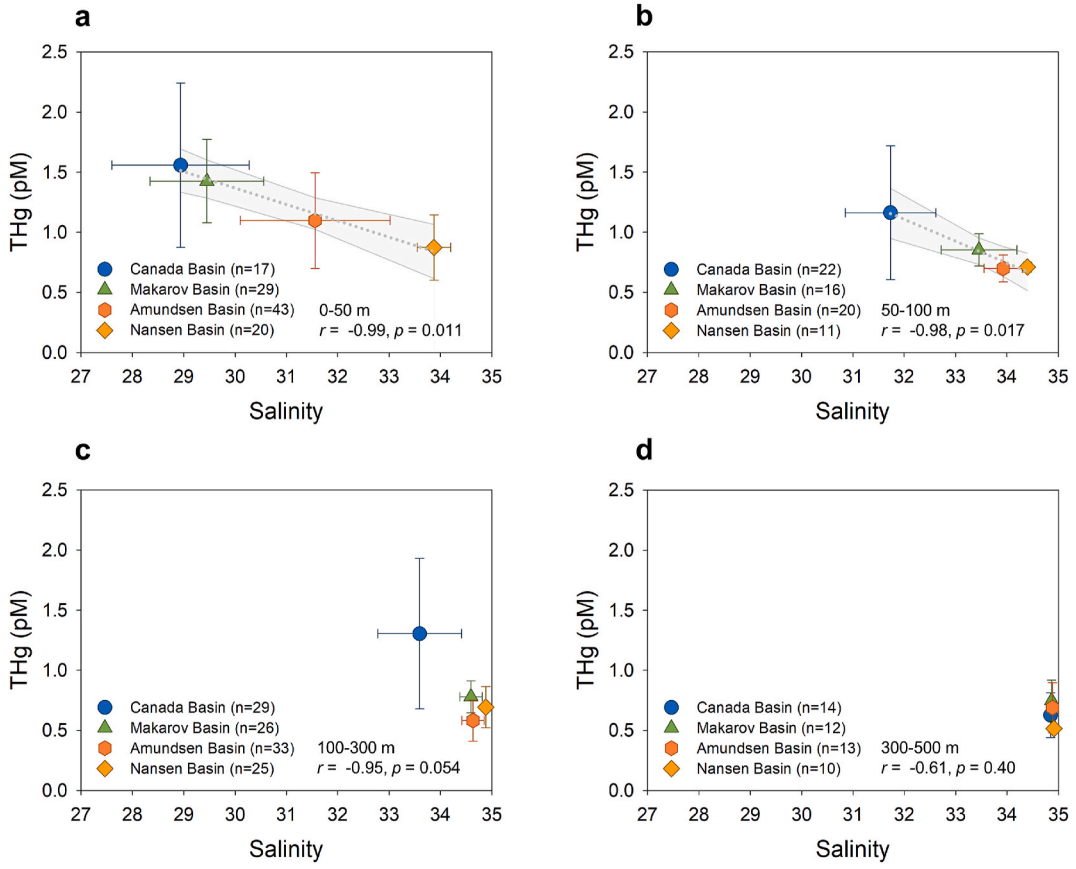

Fig. 4. Relationship between THg and salinity in (a) 0–50 m, (b) 50–100 m, (c) 100–300 m, and (d) 300–500 m of the Arctic basins. Linear regression models are shown with the best fit (dotted line) and 95 % confidence intervals (shaded). Error bars present the standard deviation of the values.

Bering Sea is 1.5 ± 0.5 pM (Fox et al., 2014), suggesting that the high THg concentration in the PW could be derived from the Chukchi Shelf, perhaps via sediment-water interactions.

The THg concentration was higher and salinity was lower in the Makarov Basin than the Atlantic sector basins at water depths of 0–50 m, while it was not clearly shown in the deeper layers (Fig. 4). This result could be attributed to the intrusion of PW into the Makarov Basin via transpolar drift, as indicated in Fig. S9. The Hg flux from major rivers and coastal erosion toward continental shelves in the Makarov Basin may additionally contribute to the increased THg concentration. In the Makarov Basin, the Hg input from river water was reported at 6.2 Mg yr^{-1} and that from coastal erosion was reported at 14.0 Mg yr^{-1} (Dastoor et al., 2022; Fabre et al., 2024) (Table S6). The THg concentration was higher and salinity was lower in the Amundsen Basin than in the Nansen Basin in the 0–50-m layer, although PW intrusion was not found in the Amundsen Basin. This may be a result of higher Hg flux from the major rivers (5.9 Mg yr^{-1}) and coastal erosion (15.0 Mg yr^{-1}) in the Amundsen Basin than the Nansen Basin (2.9 Mg yr^{-1} for rivers and 5.3 Mg yr^{-1} for coastal erosion) (Table S6). The highest salinity range (33.1–34.5) being found in the PMW of the Nansen Basin, which was mainly composed of the AW and ice meltwater, further supports the notion that freshwater runoff input is limited in the Nansen Basin (Brown et al., 2020). In fact, the sea ice meltwater fraction in the Nansen Basin was reported from −4.5 % to 5.4 % according to the GN04 survey (Paffrath et al., 2021), which explains why THg concentrations in the PMW of the Nansen Basin (0.78 ± 0.17 pM) are comparable to those in the AW (0.80 ± 0.26 pM) observed in the West Spitzbergen Current (Petrova et al., 2020).

The THg concentration in the UHW was significantly different between the Amerasian Basin and Eurasian Basin ($p < 0.05$, ANOVA; Fig. 3b) and decreased in the order: the Canada Basin (1.3 ± 0.61 pM), the Makarov Basin (1.1 ± 0.15 pM) > the Amundsen Basin (0.70 ± 0.14 pM). This corresponds to the PW intrusion in the UHW of the Canada Basin and the southern Makarov Basin, which were found to have the highest nutrient levels and the lowest N* values (Fig. S9). In accordance with this, PWW from the Chukchi Shelf has been identified as a major source of halocline water in the Canada Basin in the literature (Brugler et al., 2014; Fox et al., 2014). The PW intrusion also explains why the THg concentration in the Canada Basin is significantly ($p < 0.05$, ANOVA) higher than that in the other basins in the LHW, as PW was not able to reach to the other basins in the LHW (Fig. S9). The THg concentration in the AW was comparable between all basins.

3.5. *MeHg distribution in the Beaufort Sea*

Nutrient-type MeHg profiles were observed in the southern BS, which were mainly attributed to the photodegradation of MeHg in surface water and the *in situ* methylation of inorganic Hg(II) in subsurface water (Figs. S7e–h). The MeHg concentrations in the UPMW and LPMW were 0.066 ± 0.033 pM (n = 9) and 0.11 ± 0.049 pM (n = 11), respectively. The MeHg concentration detected for the PSW in the BS was 0.13–0.59 pM, which was similar to that found in the PSW of the Canada Basin (0.32–0.37 pM) according to the GN03 survey (Wang et al., 2018). The subsurface maxima for MeHg were primarily observed in the PWW and LHW (0.55 ± 0.074 pM, n = 8), which aligned with the previously observed peak depth of MeHg (100–300 m) in the East Siberian Sea, the Canadian Arctic Archipelago, and other Arctic basins (Jonsson et al., 2022a; Kim et al., 2020; Wang et al., 2018). MeHg concentrations in the AW decreased to 0.39 ± 0.11 pM (0.27–0.55 pM, n = 6).

In the PSW, MeHg concentrations, which showed a broader range than in the PWW and LHW, were positively correlated with BIX ($r = 0.86$

and $p = 0.002$; Fig. S11), suggesting that biologically produced DOM may promote *in situ* production of MMHg. The preferential use of phytoplankton-derived DOM, such as chlorophyll, protein, and cell wall lipids, by microbes may promote POC remineralization and Hg(II) methylation rates (Arroyo et al., 2023; Bravo et al., 2017). Moreover, detritus derived from phytoplankton may facilitate microbial aggregation. We also found that BIX and MeHg concentrations increased with temperature in the PSW (Fig. S12), as was observed for BIX in the Chukchi Sea (Chen et al., 2017). Hence, the *in situ* biological activities, positively affected by water temperature, can explain the MMHg gradients within the PSW.

In the PWW and LHW, where dissolved oxygen minima were found, MeHg concentrations were positively correlated with HIX ($r = 0.6–0.8$, $p = 0.05$; Fig. S11b). This correlation was not seen for the PSW. In the profiles from both east and west transect, the increased MeHg in the PWW is likely a result of sediment–seawater interactions (Figs. S7e–h), as was reported for dissolved Fe and humic-like DOM (Hioki et al., 2014). MeHg produced in the Canada Basin is projected to be decomposed before it reaches the southern BS based on the dark demethylation rate constant (0.36 day^{-1}) measured in the Canadian Arctic, flow velocities (0–10 cm s^{-1}), and MeHg's lifetime ($t_{1/2}$–2 day) (Lehnherr et al., 2011; Zhong et al., 2019). We consequently ascribe the positive correlation between MeHg and HIX in the PWW and LHW to the shelf sediment transport of MeHg as well as the *in situ* methylation through remineralization of POC (Kim et al., 2017; Sunderland et al., 2009). A positive correlation between humic-like DOM and MeHg concentration has been observed in the Western Pacific Ocean (Kim et al., 2017). Overall, the humic-type organic matter seems to mediate transport MeHg in addition to provide reduced substrates that can host Hg (II)-methylating microbes, such as sulfate- and iron-reducing bacteria (Sunderland et al., 2009).

3.6. Influence of Pacific water on the cross-Arctic distribution of MeHg

In the cross-Arctic MeHg comparison performed using the data from previously published expeditions, the order of the MeHg concentration in the PMW was the reverse to that observed for THg (Fig. 3b). The MeHg concentration decreased from the Atlantic to the Pacific sector in the following order: the Nansen Basin (0.16 ± 0.10 pM) > the Amundsen Basin (0.077 ± 0.041 pM) > the Makarov Basin (0.062 ± 0.033 pM) > the Canada Basin (0.035 ± 0.010 pM), with a significant difference being observed between the Nansen Basin and the other basins ($p < 0.01$, ANOVA). Biological production may play an important role in the lateral distribution of MeHg in the PMW, as indicated by the similar cross-basin trend between MeHg and Chl-a concentrations (Fig. 5). The lower biological production in the Canada, Makarov, and Amundsen Basins than the Nansen Basins appears to be related to the limited nitrate flux from the halocline water. A comparable positive relationship between Chl-a and MeHg concentration has been observed in Chukchi Sea and Antarctic seawater (Kim et al., 2020; Yue et al., 2023b).

The MeHg concentrations in the UHW and LHW were significantly higher in the Canada Basin than in other basins ($p < 0.05$; Fig. 3b), which may be attributable to the higher Hg(II) availability in the Canada Basin. The LHW in the Canada Basin has been reported as a hotspot for *in situ* microbial activity and formation of humic-like DOM (Sylvestre and Guéguen, 2024). This may contribute to produce significantly higher MeHg concentrations and MeHg/THg ratios in the LHW compared to the UHW in the Canada Basin ($p < 0.01$), as was observed in the Beaufort Sea. The MeHg concentration observed in the AW (0.37 ± 0.023 pM) was highest in the Nansen Basin, which was also four to six times higher than that reported for the AW incoming through the Fram Strait following the West Spitsbergen Current (0.09 ± 0.05 pM) and through the Barents Sea (0.06 ± 0.02 pM) (Petrova et al., 2020), supporting the previous finding that the Arctic basin is a source, rather than a sink, of MeHg (Soerensen et al., 2016a).

The MeHg/THg ratio in the PMW, representing Hg(II) methylation potential, decreased from the Atlantic to the Pacific sector in the following order: the Nansen Basin (25 ± 9.5 %) > the Amundsen Basin (6.8 ± 3.5 %) > the Makarov Basin (3.6 ± 1.4 %) > the Canada Basin (1.9 ± 0.56 %), with a statistically significant difference being observed between the Nansen basin and the other basins ($p < 0.01$; Fig. 3b). This trend supports our previous suggestion that the microbial methylation rate in the PMW follows the trend of biological production. Notably, the MeHg/THg ratio in the AW (48 ± 22 %) was higher in the Atlantic sector than the Pacific sector. This could be due to the higher microbial synthesis rate in the Atlantic sector basins, based on the contrasting profiles of temperature in the AW and Chl-a in the PMW (Fig. 3a and 5b). The higher temperature observed in the Amundsen Basin and Nansen Basin is due to the presence of a boundary current that transports warm AW into the Arctic Ocean (Våge et al., 2016).

In the Arctic basins, the MeHg/THg ratio in the upper layer (<150 m) was 25 ± 20 % (n = 106), and the MeHg/THg ratio in the intermediate layer (150–500 m) was 44 ± 20 % (n = 78). Compared to this, the MeHg/THg ratios in the upper and intermediate layers of Pacific Ocean (2.3 ± 2.4 % in the upper; 33 ± 20 % in the intermediate) (Kim et al., 2017) and Atlantic Ocean (11 ± 9 % in the upper; 17 ± 13 % in the intermediate) (Bowman et al., 2015) are considerably lower. The higher MeHg/THg ratio observed in the Arctic Ocean, despite a relatively low primary production, could be driven by the lower demethylation rate. In fact, the temperature-dependent demethylation rate constant for the polar water (0.09 yr^{-1}) was lower than those in the Pacific Ocean (0.15 yr^{-1}), which has been linked to the high sea ice extent and low temperature in the Arctic Ocean (Matilainen and Verta, 1995; Zhang et al., 2020).

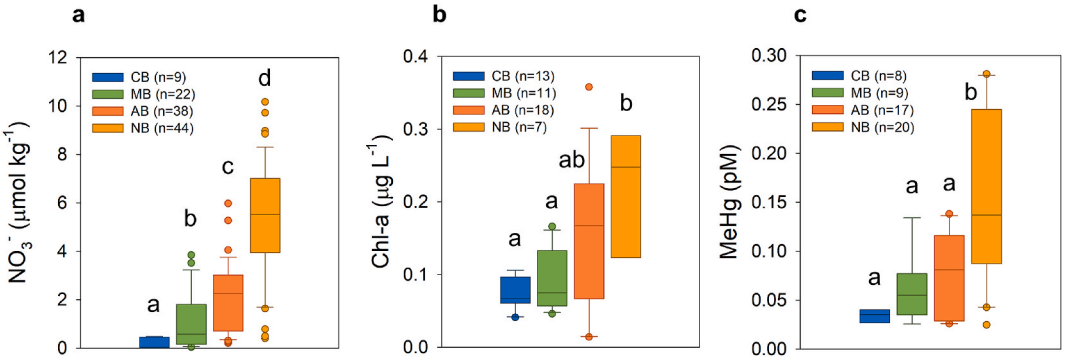

Fig. 5. Box plots showing the interquartile range (25th and 75th percentiles), median (black lines), and 10–90 % confidence interval (whiskers) for the (a) NO_3^-, (b) Chl-a concentration, and (c) MeHg in the PMW of Arctic basins. The statistically significant difference between each basin is described with a, b, and c, based on post-hoc Duncan method. Outliers are excluded using interquartile range (IQR) method. CB: Canada Basin, MB: Makarov Basin, AB: Amundsen Basin, and NB: Nansen Basin. Nitrate data were obtained from the GN01 and GIPY11 survey, and Chl-a data were obtained from the GN01, GN03, GN04 and ARK-XXVI/3 survey.

4. Conclusions

PW intrusion has traditionally been considered a minor source of THg in the Arctic Ocean, primarily due to the lower volume transport (~1 Sv) of PW as compared to AW (~9 Sv) as well as the low THg concentrations (~1.3 pM) observed in Bering Sea water (Agather et al., 2019; Petrova et al., 2020; Soerensen et al., 2016a). Our results, however, show that the PW inflow from the Chukchi Sea significantly elevates THg concentrations in the PMW and halocline water of the Canada Basin. In the PMW, a gradual decline of THg from the Canada Basin to the Nansen Basin through the Makarov Basin and Amundsen Basin was observed along with a gradual increase of salinity, which can be linked to the higher Hg input from runoff water and coastal erosion in the Makarov and Amundsen Basin than the Nansen Basin, as well as PW intrusion to the Canada and Makarov Basin. THg concentrations in the AW were comparable between all basins. While the vertical MeHg profiles in the Arctic Ocean have been attributed to *in situ* production and decomposition, the factors influencing the spatial variability of MeHg concentrations across the Arctic basins are not well understood. We show that the highest Hg(II) availability results in the highest MeHg concentration in the halocline water in the Canada Basin. In the PMW, the MeHg concentration significantly increased in the Nansen Basin, which corresponds to the cross-basin trend for Chl-a concentration driven by the high nitrate availability in the Nansen Basin. In the AW, significantly higher MeHg concentrations were observed in the Nansen Basin compared to other basins, possibly due to the increased microbial activities under the high seawater temperature and biological production in the Nansen Basin. In conclusion, our study highlights the critical role of PW and AW inflows in modulating the lateral and vertical profiles of THg and MeHg in the Arctic Ocean.

From 1990 to 2019, the Pacific sector of the Arctic Ocean experienced warming at a rate of 0.05 °C per year and freshening at a rate of 0.03 per year, which is attributable to an increase in PW inflow at a rate of 0.01 Sv per year (Woodgate and Peralta-Ferriz, 2021). These changes are likely to increase THg concentrations in the Pacific sector, as the intrusion of low-salinity Chukchi Sea water contributes to THg transport. Additionally, a notable increase in temperature was observed in the PSW in the Canada Basin from 2006 to 2020, with temperature further increasing as one moves toward the PMW (MacKinnon et al., 2021; Timmermans and Toole, 2023; Woodgate, 2018). This shift is linked to the increased heat flux associated with sea ice melting in the Chukchi Sea. Such conditions may increase the availability of MeHg to low-trophic organisms in the PMW and shallow subsurface seawater (Wang et al., 2018). In the Atlantic sector, the increased inflow of seawater from the Nordic Seas, driven by the atmospheric Arctic dipole, indicates Arctic seawater's transition to a state resembling that of Atlantic Ocean water, a process referred as atlantification (Ingvaldsen et al., 2021; Polyakov et al., 2023). From 2007 to 2021, the inflow of AW through the Barents Sea increased, while inflow through the Fram Strait decreased in the upper 50 m, correlating with the shift in atmospheric cyclones over the Barents Sea (Polyakov et al., 2023). Given that THg concentrations in the Barents Sea are approximately half those in the Fram Strait (Petrova et al., 2020), atlantification may lead to a decrease in THg concentrations in the Atlantic sector. Overall, the alterations in physical and biogeochemical conditions of Arctic Ocean waters due to climate change are anticipated to influence Hg cycling, potentially intensifying the difference in THg and MeHg concentrations between the Pacific and Atlantic sectors.

CRediT authorship contribution statement

Sangwoo Eom: Writing – original draft, Investigation, Data curation. **Anne L. Soerensen:** Writing – review & editing, Visualization, Validation. **Tae Siek Rhee:** Writing – review & editing, Investigation, Formal analysis. **Jong Kuk Hong:** Validation, Project administration, Data curation. **Purena Son:** Investigation, Formal analysis, Data curation. **Tae Keun Rho:** Validation, Formal analysis, Data curation. **Seunghee Han:** Writing – review & editing, Supervision, Funding acquisition, Conceptualization.

Declaration of competing interest

The authors declare that they have no known competing financial interests or personal relationships that could have appeared to influence the work reported in this paper.

Acknowledgment

This study was funded by the Ministry of Oceans and Fisheries through the Open Innovation Project (RS-2021-KS211487) and National Research Foundation of Korea (RS-2024-00454238). We thank all the researchers participated in the previous Arctic expeditions for making their data publicly available.

Appendix A. Supplementary data

Supplementary data to this article can be found online at https://doi.org/10.1016/j.envpol.2025.126254.

Data availability

Data will be made available on request.

References

Agather, A.M., Bowman, K.L., Lamborg, C.H., Hammerschmidt, C.R., 2019. Distribution of mercury species in the Western Arctic Ocean (US GEOTRACES GN01). Mar. Chem. 216, 103686.
Aksenov, Y., Karcher, M., Proshutinsky, A., Gerdes, R., De Cuevas, B., Golubeva, E., Kauker, F., Nguyen, A.T., Platov, G.A., Wadley, M., 2016. Arctic pathways of Pacific Water: arctic Ocean M odel I intercomparison experiments. J. Geophys. Res. Oceans 121, 27–59.
Alkire, M.B., Falkner, K.K., Morison, J., Collier, R.W., Guay, C.K., Desiderio, R.A., Rigor, I.G., McPhee, M., 2010. Sensor-based profiles of the NO parameter in the central Arctic and southern Canada Basin: new insights regarding the cold halocline. Deep-Sea Res. PT I. 57, 1432–1443.
Andersson, M., Sommar, J., Gårdfeldt, K., Lindqvist, O., 2008. Enhanced concentrations of dissolved gaseous mercury in the surface waters of the Arctic Ocean. Mar. Chem. 110, 190–194.
Arroyo, A., Timmermans, M.L., Le Bras, I., Williams, W., Zimmermann, S., 2023. Declining O2 in the Canada Basin halocline consistent with physical and biogeochemical effects of Pacific summer water warming. J. Geophys. Res. Oceans 128, e2022JC019418.
Basu, N., Abass, K., Dietz, R., Krümmel, E., Rautio, A., Weihe, P., 2022. The impact of mercury contamination on human health in the Arctic: a state of the science review. Sci. Total Environ. 831, 154793.
Baya, P.A., Gosselin, M., Lehnherr, I., St Louis, V.L., Hintelmann, H., 2015. Determination of monomethylmercury and dimethylmercury in the Arctic marine boundary layer. Environ. Sci. Technol. 49, 223–232.
Black, F.J., Conaway, C.H., Flegal, A.R., 2009. Stability of dimethyl mercury in seawater and its conversion to monomethyl mercury. Environ. Sci. Technol. 43, 4056–4062.
Bluhm, B., Kosobokova, K., Carmack, E., 2015. A tale of two basins: an integrated physical and biological perspective of the deep Arctic Ocean. Prog. Oceanogr. 139, 89–121.
Bowman, K.L., Hammerschmidt, C.R., Lamborg, C.H., Swarr, G., 2015. Mercury in the North Atlantic Ocean: the US GEOTRACES zonal and meridional sections. Deep-Sea Res. PT II 116, 251–261.
Bravo, A.G., Bouchet, S., Tolu, J., Björn, E., Mateos-Rivera, A., Bertilsson, S., 2017. Molecular composition of organic matter controls methylmercury formation in boreal lakes. Nat. Commun. 8, 14255.
Brown, K.A., Holding, J.M., Carmack, E.C., 2020. Understanding regional and seasonal variability is key to gaining a pan-Arctic perspective on Arctic Ocean freshening. Front. Mar. Sci. 7, 606.
Brugler, E.T., Pickart, R.S., Moore, G., Roberts, S., Weingartner, T.J., Statscewich, H., 2014. Seasonal to interannual variability of the Pacific water boundary current in the Beaufort Sea. Prog. Oceanogr. 127, 1–20.
Chaudhary, D.K., Seo, D., Han, S., Hong, Y., 2024. Distribution of mercury in modern bottom sediments of the Beaufort Sea in relation to the processes of early diagenesis: microbiological aspect. Mar. Pollut. Bull. 202, 116300.
Chen, M., Nam, S.-I., Kim, J.-H., Kwon, Y.-J., Hong, S., Jung, J., Shin, K.-H., Hur, J., 2017. High abundance of protein-like fluorescence in the Amerasian Basin of Arctic Ocean: potential implication of a fall phytoplankton bloom. Sci. Total Environ. 599, 355–363.

Codispoti, L., Kelly, V., Thessen, A., Matrai, P., Suttles, S., Hill, V., Steele, M., Light, B., 2013. Synthesis of primary production in the Arctic Ocean: III. Nitrate and phosphate based estimates of net community production. Prog. Oceanogr. 110, 126–150.
Dabrowski, J.S., Pickart, R.S., Stockwell, D.A., Lin, P., Charette, M.A., 2022. Physical drivers of sediment-water interaction on the Beaufort Sea shelf. Deep-Sea Res. PT I 181, 103700.
Dastoor, A., Angot, H., Bieser, J., Christensen, J.H., Douglas, T.A., Heimbürger-Boavida, L.-E., Jiskra, M., Mason, R.P., McLagan, D.S., Obrist, D., 2022. Arctic mercury cycling. Nat. Rev. Earth Environ. 3, 270–286.
DeFrancesco, C., Guéguen, C., Williams, W., Zimmermann, S., 2023. Interannual variability of fluorescent dissolved organic matter composition in the Canada Basin, Arctic Ocean from 2007 to 2017. J. Geophys. Res. Oceans 128, e2022JC018919.
DiMento, B.P., Mason, R.P., Brooks, S., Moore, C., 2019. The impact of sea ice on the air-sea exchange of mercury in the Arctic Ocean. Deep-Sea Res. PT I. 144, 28–38.
Ehn, J.K., Reynolds, R.A., Stramski, D., Doxaran, D., Lansard, B., Babin, M., 2019. Patterns of suspended particulate matter across the continental margin in the Canadian Beaufort Sea during summer. Biogeosciences 16, 1583–1605.
Emmerton, C.A., Graydon, J.A., Gareis, J.A., St Louis, V.L., Lesack, L.F., Banack, J.K., Hicks, F., Nafziger, J., 2013. Mercury export to the Arctic ocean from the Mackenzie River, Canada. Environ. Sci. Technol. 47, 7644–7654.
Eom, S., Kim, J., Jung, E., Kwon, S.Y., Hong, Y., Lee, M., Park, J.H., Han, S., 2024. Effects of hydrologic regimes on the loading and spatiotemporal variation of mercury in the microtidal river estuary. Mar. Pollut. Bull. 205, 116602.
Fabre, C., Sonke, J.E., Tananaev, N., Teisserenc, R., 2024. Organic carbon and mercury exports from pan-Arctic rivers in a thawing permafrost context–A review. Sci. Total Environ., 176713
Fox, A.L., Hughes, E.A., Trocine, R.P., Trefry, J.H., Schonberg, S.V., McTigue, N.D., Lasorsa, B.K., Konar, B., Cooper, L.W., 2014. Mercury in the northeastern Chukchi Sea: distribution patterns in seawater and sediments and biomagnification in the benthic food web. Deep-Sea Res. PT II 102, 56–67.
Graydon, J.A., Emmerton, C.A., Lesack, L.F., Kelly, E.N., 2009. Mercury in the Mackenzie River Delta and Estuary: concentrations and fluxes during open-water conditions. Sci. Total Environ. 407, 2980–2988.
Hansen, A.M., Kraus, T.E., Pellerin, B.A., Fleck, J.A., Downing, B.D., Bergamaschi, B.A., 2016. Optical properties of dissolved organic matter (DOM): effects of biological and photolytic degradation. Limnol. Oceanogr. 61, 1015–1032.
Heimbürger, L.-E., Sonke, J.E., Cossa, D., Point, D., Lagane, C., Laffont, L., Galfond, B.T., Nicolaus, M., Rabe, B., van Der Loeff, M.R., 2015. Shallow methylmercury production in the marginal sea ice zone of the central Arctic Ocean. Sci. Rep. 5, 10318.
Hioki, N., Kuma, K., Morita, Y., Sasayama, R., Ooki, A., Kondo, Y., Obata, H., Nishioka, J., Yamashita, Y., Nishino, S., 2014. Laterally spreading iron, humic-like dissolved organic matter and nutrients in cold, dense subsurface water of the Arctic Ocean. Sci. Rep. 4, 6775.
Ingvaldsen, R.B., Assmann, K.M., Primicerio, R., Fossheim, M., Polyakov, I.V., Dolgov, A. V., 2021. Physical manifestations and ecological implications of Arctic Atlantification. Nat. Rev. Earth Environ. 2, 874–889.
Jonsson, S., Mastromonaco, M.G.N., Gårdfeldt, K., Mason, R.P., 2022a. Distribution of total mercury and methylated mercury species in Central Arctic Ocean water and ice. Mar. Chem. 242, 104105.
Jonsson, S., Mastromonaco, M.N., Wang, F., Bravo, A.G., Cairns, W.R., Chételat, J., Douglas, T.A., Lescord, G., Ukonmaanaho, L., Heimbürger-Boavida, L.-E., 2022b. Arctic methylmercury cycling. Sci. Total Environ. 850, 157445.
Kim, H., Soerensen, A.L., Hur, J., Heimburger, L.-E., Hahm, D., Rhee, T.S., Noh, S., Han, S., 2017. Methylmercury mass budgets and distribution characteristics in the Western Pacific Ocean. Environ. Sci. Technol. 51, 1186–1194.
Kim, J., Moon, J.-K., Yang, E.J., Kim, E., Han, S., 2023. Sources and melt flux of methylmercury in sea ice on the Chukchi Plateau, Arctic Ocean. Estuar. Coast Shelf Sci. 294, 108536.
Kim, J., Soerensen, A.L., Kim, M.S., Eom, S., Rhee, T.S., Jin, Y.K., Han, S., 2020. Mass budget of methylmercury in the East Siberian Sea: the importance of sediment sources. Environ. Sci. Technol. 54, 9949–9957.
Kohler, S.G., Heimbürger-Boavida, L.-E., Petrova, M.V., Digernes, M.G., Sanchez, N., Dufour, A., Simić, A., Ndungu, K., Ardelan, M.V., 2022. Arctic Ocean's wintertime mercury concentrations limited by seasonal loss on the shelf. Nat. Geosci. 15, 621–626.
Lavoie, R.A., Jardine, T.D., Chumchal, M.M., Kidd, K.A., Campbell, L.M., 2013. Biomagnification of mercury in aquatic food webs: a worldwide meta-analysis. Environ. Sci. Technol. 47, 13385–13394.
Lehnherr, I., St Louis, V.L., Hintelmann, H., Kirk, J.L., 2011. Methylation of inorganic mercury in polar marine waters. Nat. Geosci. 4, 298–302.
Liguori, B.T., Ehlert, C., Nöthig, E.M., van Ooijen, J.C., Pahnke, K., 2021. The transpolar drift influence on the Arctic Ocean silicon cycle. J. Geophys. Res. Oceans 126, e2021JC017352.
Lin, P., Pickart, R.S., Weingartner, T.J., Simmons, H.L., Itoh, M., Kikuchi, T., 2023. Formation and circulation of newly ventilated winter water in the western Beaufort Sea. Prog. Oceanogr. 216, 103068.
MacKinnon, J.A., Simmons, H.L., Hargrove, J., Thomson, J., Peacock, T., Alford, M.H., Barton, B.I., Boury, S., Brenner, S.D., Couto, N., 2021. A warm jet in a cold ocean. Nat. Commun. 12, 2418.
Matilainen, T., Verta, M., 1995. Mercury methylation and demethylation in aerobic surface waters. Can. J. Fish. Aquat. Sci. 52, 1597–1608.
Matsuoka, A., Bricaud, A., Benner, R., Para, J., Sempéré, R., Prieur, L., Bélanger, S., Babin, M., 2012. Tracing the transport of colored dissolved organic matter in water masses of the Southern Beaufort Sea: relationship with hydrographic characteristics. Biogeosciences 9, 925–940.
Paffrath, R., Laukert, G., Bauch, D., Rutgers van der Loeff, M., Pahnke, K., 2021. Separating individual contributions of major Siberian rivers in the transpolar drift of the Arctic Ocean. Sci. Rep. 11, 8216.
Pasqualini, A., Schlosser, P., Newton, R., Koffman, T., 2017. US GEOTRACES Arctic section ocean water hydrogen and oxygen stable isotope analyses. Version 1.0. Interdisciplinary Earth Data Alliance (IEDA).
Peralta-Ferriz, C., Woodgate, R.A., 2015. Seasonal and interannual variability of pan-arctic surface mixed layer properties from 1979 to 2012 from hydrographic data, and the dominance of stratification for multiyear mixed layer depth shoaling. Prog. Oceanogr. 134, 19–53.
Petrova, M.V., Krisch, S., Lodeiro, P., Valk, O., Dufour, A., Rijkenberg, M.J., Achterberg, E.P., Rabe, B., van der Loeff, M.R., Hamelin, B., 2020. Mercury species export from the Arctic to the Atlantic Ocean. Mar. Chem. 225, 103855.
Polyakov, I.V., Ingvaldsen, R.B., Pnyushkov, A.V., Bhatt, U.S., Francis, J.A., Janout, M., Kwok, R., Skagseth, Ø., 2023. Fluctuating Atlantic inflows modulate Arctic atlantification. Science 381, 972–979.
Qi, Y., Yang, Q., Yamagata, T., Matsuzaki, H., Nagai, H., Kumamoto, Y., Itoh, M., 2024. Anthropogenic iodine-129 tracks iodine cycling in the Arctic. Geochem. Cosmochim. Acta.
Randelhoff, A., Holding, J., Janout, M., Sejr, M.K., Babin, M., Tremblay, J.-É., Alkire, M. B., 2020. Pan-Arctic ocean primary production constrained by turbulent nitrate fluxes. Front. Mar. Sci. 7, 150.
Rudels, B., Carmack, E., 2022. Arctic Ocean water mass structure and circulation. Oceanography. 35, 52–65.
Saniewska, D., Bełdowska, M., Szymczak, E., Kuliński, K., Bełdowski, J., Voss, M., Pryputniewicz-Flis, D., Burska, D., 2022. Processes affecting the transformation of mercury in the coastal zone in the vicinity of two river mouths in the southern Baltic Sea. Mar. Chem. 238, 104065.
Schlitzer, R., Mieruch-Schnülle, S., 2024. The GEOTRACES intermediate data products. Oceanography. 37, 25–33.
Soerensen, A.L., Jacob, D.J., Schartup, A.T., Fisher, J.A., Lehnherr, I., St Louis, V.L., Heimbürger, L.E., Sonke, J.E., Krabbenhoft, D.P., Sunderland, E.M., 2016a. A mass budget for mercury and methylmercury in the Arctic Ocean. Glob. Biogeochem. Cycles 30, 560–575.
Soerensen, A.L., Schartup, A.T., Gustafsson, E., Gustafsson, B.G., Undeman, E., Bjorn, E., 2016b. Eutrophication increases phytoplankton methylmercury concentrations in a coastal sea A Baltic Sea Case ctudy. Environ. Sci. Technol. 50, 11787–11796.
Stedmon, C.A., Bro, R., 2008. Characterizing dissolved organic matter fluorescence with parallel factor analysis: a tutorial. Limnol Oceanogr. Methods 6, 572–579.
Stedmon, C.A., Markager, S., Bro, R., 2003. Tracing dissolved organic matter in aquatic environments using a new approach to fluorescence spectroscopy. Mar. Chem. 82, 239–254.
Streit, M., Gehlenborg, N., 2014. Points of view: bar charts and box plots. Nat. Methods 11.
Sunderland, E.M., Krabbenhoft, D.P., Moreau, J.W., Strode, S.A., Landing, W.M., 2009. Mercury sources, distribution, and bioavailability in the North Pacific Ocean: insights from data and models. Glob. Biogeochem. Cycles 23.
Sylvestre, N., Guéguen, C., 2024. Influence of microbial activities on fluorescent dissolved organic matter in the dark Canada Basin waters. J. Geophys. Res. Oceans 129, e2023JC020603.
Timmermans, M.-L., Toole, J.M., 2023. The Arctic Ocean's beaufort gyre. Ann. Rev. Mar. Sci 15, 223–248.
Våge, K., Pickart, R.S., Pavlov, V., Lin, P., Torres, D.J., Ingvaldsen, R., Sundfjord, A., Proshutinsky, A., 2016. The Atlantic W ater boundary current in the Nansen Basin: transport and mechanisms of lateral exchange. J. Geophys. Res. Oceans 121, 6946–6960.
Wang, K., Munson, K.M., Beaupré-Laperrière, A., Mucci, A., Macdonald, R.W., Wang, F., 2018. Subsurface seawater methylmercury maximum explains biotic mercury concentrations in the Canadian Arctic. Sci. Rep. 8, 1–5.
West, J., Babi, D., Azaroff, A., Jonsson, S., 2023. Dimethylmercury in natural waters—analytical and experimental considerations. Limnol Oceanogr. Methods 21, 837–846.
Woodgate, R.A., 2018. Increases in the Pacific inflow to the Arctic from 1990 to 2015, and insights into seasonal trends and driving mechanisms from year-round Bering Strait mooring data. Prog. Oceanogr. 160, 124–154.
Woodgate, R.A., Peralta-Ferriz, C., 2021. Warming and Freshening of the Pacific Inflow to the Arctic from 1990-2019 implying dramatic shoaling in Pacific winter water ventilation of the Arctic water column. Geophys. Res. Lett. 48, e2021GL092528.
Yue, F., Angot, H., Blomquist, B., Schmale, J., Hoppe, C.J., Lei, R., Shupe, M.D., Zhan, L., Ren, J., Liu, H., 2023a. The marginal ice zone as a dominant source region of atmospheric mercury during central Arctic summertime. Nat. Commun. 14, 4887.
Yue, F., Li, Y., Zhang, Y., Wang, L., Li, D., Wu, P., Liu, H., Lin, L., Li, D., Hu, J., 2023b. Elevated methylmercury in Antarctic surface seawater: the role of phytoplankton mass and sea ice. Sci. Total Environ. 882, 163646.
Zhang, Y., Soerensen, A.L., Schartup, A.T., Sunderland, E.M., 2020. A global model for methylmercury formation and uptake at the base of marine food webs. Glob. Biogeochem. Cycles 34, e2019GB006348.
Zhong, W., Steele, M., Zhang, J., Cole, S.T., 2019. Circulation of Pacific winter water in the Western Arctic Ocean. J. Geophys. Res. Oceans 124, 863–881.
Zolkos, S., Krabbenhoft, D.P., Suslova, A., Tank, S.E., McClelland, J.W., Spencer, R.G., Shiklomanov, A., Zhulidov, A.V., Gurtovaya, T., Zimov, N., 2020. Mercury export from Arctic great rivers. Environ. Sci. Technol. 54, 4140–4148.